**International Journal in Physical and Applied Sciences**
Volume 06 Issue 02, February 2019 ISSN: 2394-5710 Impact Factor: 4.657
Journal Homepage: http://ijmr.net.in, Email: irjmss@gmail.com
Double-Blind Peer Reviewed Refereed Open Access International Journal

# Ion traps on rotating radio frequencies.

Anil kumar[1*], Manish Kumar[2], Dr. Bishwa Mohan kumar[3]
[1,2,3] Magadh University, Bodhgaya,824234,india
Email. : teacheranil78@gmail.com

## Abstracts

In this article, we explore the rotating-radio-frequency rotating-rf trap, a radio-frequency rf ion trap in which the motion of a charged particle is represented by trigonometric functions as opposed to the typical Mathieu functions of a conventional rf trap. Charged particles are contained in the rotating-rf trap by a revolving quadrupole electric field, as opposed to an oscillating quadrupole electric field in a standard rf trap. Two no degenerate circular secular movements and two related circular micromotions combine to form the ion motion in a rotating-rf trap. In addition to the rotating-rf field, instances of applying a uniform dc magnetic field or a quadrupole dc electric field are also covered. With the same experimental parameter values, confinement in a rotating-rf trap may be tighter than in a standard linear-rf trap.

Keyword- radio-frequency, Paul ion trap

## 1. **INTRODUCTION.**

Ion traps are frequently utilized in a wide range of applications. Studies on quantum computing are examples.[1-4] high-resolution spectroscopy and atomic clocks.[5-9], non neutral-plasma physics [10-14] Applications where a strong magnetic field is neither required or desired can benefit greatly from the usage of the rf or Paul ion trap. Rf traps, for instance, have been used to carefully examine the interaction of atoms with light in atomic physics and quantum optics.[17-19]. Paul created the rf trap, a three-dimensional variation of his magnetic-field-free mass spectrometer, in the 1950s.[15] utilizes an inhomogeneous, oscillating rf electric field to create a force that confines charged particles.[20] The functioning of an rf trap has been described using a rotating-saddle potential.[21] The gravitational saddle-shaped potential in a rotating-saddle trap revolves around a gravity axis, but the electric saddle-shaped potential in an rf trap oscillates or "flaps" with the rf drive frequency. As a result, the rotating-saddle trap is not a precise mechanical counterpart of the rf trap.[22]. It turns out that trigonometric functions can adequately explain the motion of a ball in a rotating-saddle trap. in contrast to those in a rf trap, which are described by Mathieu functions [15,23,2441].As a result, it makes sense to assume that the motion of a charged particle in an electric variant of the rotating-

saddle trap may similarly be explained by trigonometric functions and could even be simpler than that in a typical rf trap. Some of the applications and investigations that employ rf traps may benefit from simpler ion motion. ions and research that employs rf traps. The rotating-saddle trap, an electric adaptation, is the subject of this paper's discussion. The trap comprises of a rotating quadrupole electric field for confinement in the orthogonal radial directions and a dc electric field for confinement in one direction, z. The linear rf lrf trap, which is widely used, and the rotating-rf rrf trap are comparable[5]. The rrf trap's rf quadrupole electric field rotates as opposed to the lrf trap's oscillating rf quadrupole electric field. By applying sinusoidal voltages with various phases to six or more electrodes that are positioned azimuthally around the trap, it is possible to create a spinning quadrupole electric field. This technique, commonly referred to as a revolving wall, has been used to create a rotating electric field in a Penning trap in order to regulate the plasma rotation frequency.[25,26].

## II. STABILITY OF ROTATING-rf TRAPS:

A static electric potential (Z) for axial confinement and a spinning electric potential (R) for radial confinement make up a rrf trap. They are written as

$$\phi_z = -\,Vd/\,r_d{}^2\,(r^2 - 2z^2)\,,$$
$$\phi_r = Vr/\,r^2{}_r\;\; r^2\cos[2(\theta + \omega t\,] \qquad (1)$$

Here, the electrodes' effective dimensions, which take into account their geometric properties, are given by $r_d$ and $r_r$, while the particle's location in cylindrical coordinates is described by r,θ, z, and. Vd and Vr are theω rotating and direct current voltages. In the remaining sections of this work, we implicitly assume that 0 and positive ω equate to rotation in the –θ direction. Electrodes like those in Fig. 1 can be used to supply the potentials in Eq. 1. Each of the six rod electrodes in Fig. 1 receives an application of a sinusoidal voltage with a certain phase. This voltage has an angular frequency of 2ω. In addition to the quadrupole field revolving with frequency, the setup of Fig. 1 may also produce an octupole field spinning with frequency and higher-order fields. At the center of the trap, however, the contribution of the quadrupole field is dominant

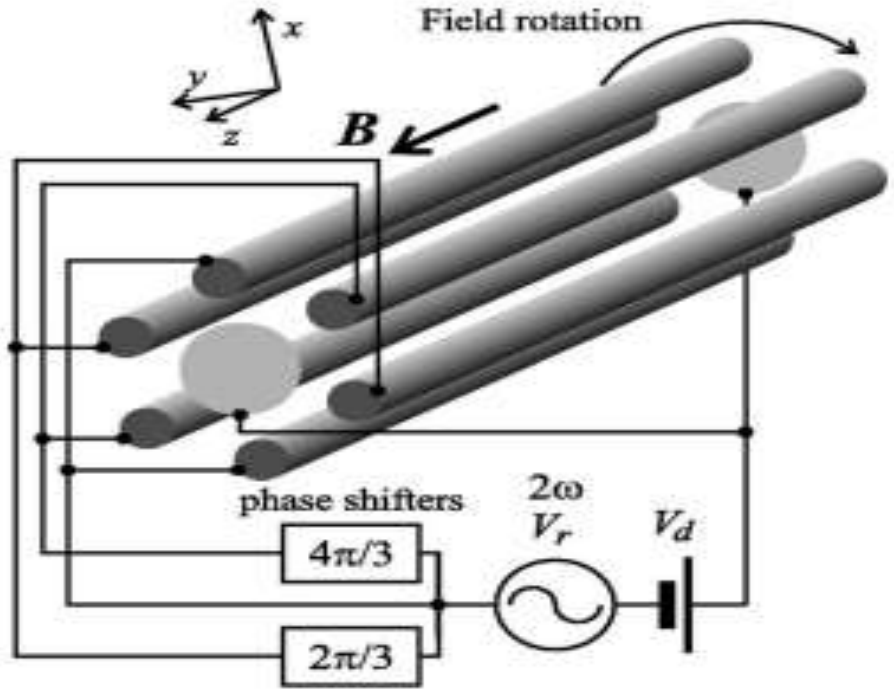


FIG. 1. A possible experimental realization of a rrf trap. The phase shifters delay the ac voltage by the shown phase; namely, if the input of the 2π/ 3 phase shifter is V cos 2ωt, the output is V cos (2ωt− 2π/ 343)

In addition to the quadrupole field revolving with frequency, the setup of Fig. 1 may also produce an octupole field spinning with frequency. Due to the octupole field's spatial dependency being proportional to r4, the quadrupole field's contribution is dominating. We additionally take into account a uniform magnetic field B pointing in the z direction in addition to the fields of Eq(1)
The equations of motion can be written as

$$\frac{d^2x}{d\tau^2} = \mu\frac{dy}{d\tau} + dx - 2q(x\cos 2\tau - y\sin 2\tau), \qquad (2)$$

$$\frac{d^2y}{d\tau^2} = -\mu\frac{dx}{d\tau} + dy + 2q(x\sin 2\tau + y\cos 2\tau), \qquad (3)$$

$$\frac{d^2z}{d\tau^2} = -2dz. \qquad (4)$$

Here, τ=ωt, =Ω=eB/m is the cyclotron frequency, d = 2eVd /mrd 2 2 , q=eVr/mr$^2$ r$^2$ , and m and e are the mass and charge of the particle, respectively.τ,μ, d, and q are dimensionless. By selecting positive d, axial confinement with axial frequency z=2d is produced. Therefore, we must only talk about the requirements for stable confinement in the radial direction. Although q's value might be positive or negative, its physical sign solely relies on how the x and y axes are selected. As a result, the stability of the trap is unaffected by the sign of q. In this essay, we shall contrast the rrf trap to the lrf trap. We examine a lrf trap whose rf "flapping" potential is provided by and whose static electric potential is the same as Ω in Eq.(5)

$$\Phi_{\text{lrf}} = \frac{V_r}{r_r^2} r^2 \cos(2\theta)\cos(2\omega t). \qquad (5)$$

A typical four-rod trap arrangement with the same size and rf voltage amplitude as the rrf trap mentioned above may produce this potential. The 2qy sin 2τ term in Eq. 2 and the 2qx sin 2 term in Eq. 3 are absent from the equations of motion for the lrf trap, which are otherwise the same as Eqs. (2 and 4). By inserting new coordinates a z, in a frame rotating with frequency, defined by (Ref. 27), Eqs. 2 and 3 may be solved analytically with no approximations.

$$x = \xi \cos\tau + \zeta \sin\tau,$$

$$y = \zeta \cos\tau - \xi \sin\tau. \qquad (6)$$

The solution in the rotating frame is

$$\xi = \sum_{j=1}^{2} (C_j e^{i\lambda_j \tau} + D_j e^{-i\lambda_j \tau}),$$

$$\zeta = \sum_{j=1}^{2} i \frac{\lambda_j^2 - \mu + d + 1 - 2q}{\lambda_j(\mu - 2)} (C_j e^{i\lambda_j \tau} - D_j e^{-i\lambda_j \tau}), \qquad (7)$$

Where *Cj* and *Dj* are constants determined by the initial conditions, and the _*j* are given by

$$\lambda_1 = \left[\mu - d - 1 + \tfrac{1}{2}(\mu-2)^2 + \tfrac{1}{2}\sqrt{(\mu-2)^2(\mu^2-4d)+16q^2}\right]^{1/2}$$

$$\lambda_2 = \left[\mu - d - 1 + \tfrac{1}{2}(\mu-2)^2 - \tfrac{1}{2}\sqrt{(\mu-2)^2(\mu^2-4d)+16q^2}\right]^{1/2}. \quad (8)$$

The solutions to Eq. 7 diverge rapidly and the trap becomes unstable if the j has a nonzero imaginary portion. The trap is stable if the j are real valued numbers. Real j requires the simultaneous fulfilment of the following conditions:

$$(\mu-2)^2(\mu^2-4d)+16q^2 > 0,$$

$$\mu - d - 1 + \tfrac{1}{2}(\mu-2)^2 - \tfrac{1}{2}\sqrt{(\mu-2)^2(\mu^2-4d)+16q^2} > 0. \quad (9)$$

Cj and Dj must be complex conjugates of one another for real-valued j since is a real variable. Real is inherently valued under this circumstance. In this instance, the laboratory frame's solutions change into

$$x = \sum_{j=1,2} [(1-\gamma_j)A_j \cos(\omega_{j+}\tau + \phi_j) + (1+\gamma_j)A_j \cos(\omega_{j-}\tau - \phi_j)],$$

$$y = \sum_{j=1,2} [(1-\gamma_j)A_j \sin(\omega_{j+}\tau + \phi_j) + (1+\gamma_j)A_j \sin(\omega_{j-}\tau - \phi_j)], \quad (10)$$

where *Ajeij=Cj=Dj* * , _j=__j 2 −_ +*d*+1−2*q*_ / __j__ −2__, and _j±=−1±_j _j=1,2_ are the normalized characteristic frequencies of the trapped particle motion in the laboratory frame

We see that j=2j+. Equation 10 demonstrates that the characteristic movements are circular and that the sign of the eigenfrequencies determines the direction of their rotation. The stability requirement of Eq. 9 changes when a rrf trap is involved since there is no magnetic field and =0.

$$\mathbf{d < q^2}$$

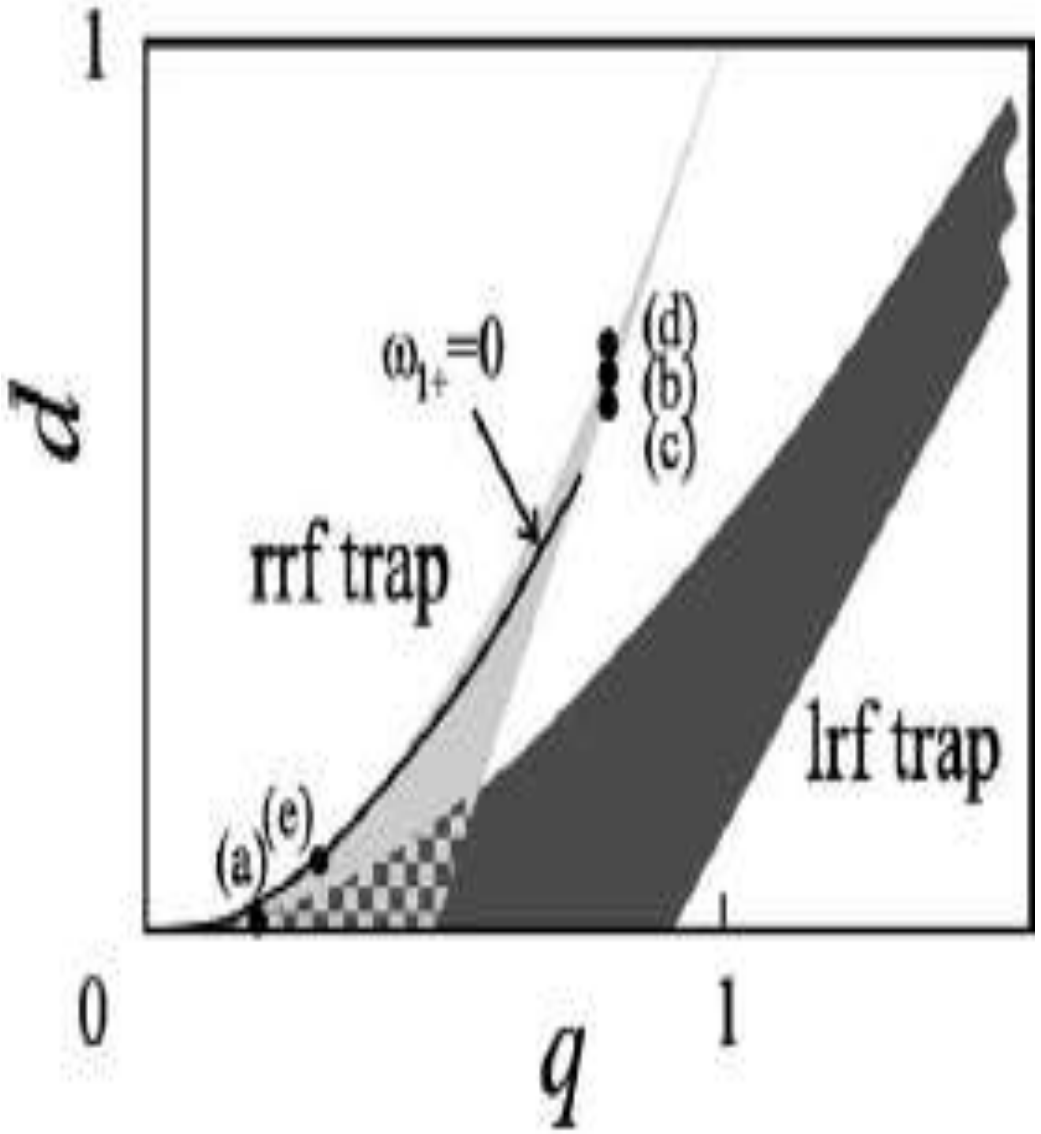


FIG. 2. Stability diagrams in the *q*-*d* plane for μ =0 of a rrf and a lrf trap

The lrf trap's stability area widens as q and d get bigger, but it also gets progressively narrower. The stable area for both traps is the checked area. The black dots in Fig. 3 represent the values of the parameters utilised there. The parameter values shown by the line cause one of the secular frequencies 1+ to become zero.

$$d > 2|q| - 1$$

$$d < 1 \quad \ldots\ldots\ldots\ldots\ldots\ldots\ldots\ldots\ldots\ldots (11)$$

Stability in the z direction also depends on the presence of the condition of d0. Figure 2 28 compares the low-order stability area of a lrf trap with the stability diagram of a rrf trap. For a rrf trap, there is just one stability zone, and it is smaller in size than the stability region for a lrf trap.

.With μ =0, the eigenfrequencies of Eq. (8) become:

$$\lambda_1 = (1 - d + 2\sqrt{q^2 - d})^{1/2},$$

$$\lambda_2 = (1 - d - 2\sqrt{q^2 - d})^{1/2}, \qquad (12)$$

$$\omega_{1\pm} = -1 \pm (1 - d + 2\sqrt{q^2 - d})^{1/2},$$

$$\omega_{2\pm} = -1 \pm (1 - d - 2\sqrt{q^2 - d})^{1/2}. \qquad (13)$$

ω1 and ω2 are always negative and represent circular motion in the same direction as the rotating potential when applied. For a trap with weak axial confinement d>>q, ω1+ can be of either sign, but it always indicates positive circular motion contrary to the applied rotating potential. Therefore in general the radial motion is composed of circular components rotating in both directions .For the special case $d$=−2+2 ( 1+$q$2 )$^{1/2}$

One benefit of a rrf trap is that the radial motion has only four Fourier components, as opposed to an infinite number in a lrf trap, where the radial motion is described by Mathieu functions and the Fourier components are nrfsecular, where μrf is the applied rf frequency, secular is the secular frequency, and n is any integer. Because there are less motional sidebands in the rrf trap compared to the lrf trap, for instance, the optical spectral lines of energetic ions may be simpler.

Fig. 3 displays a few illustrations of particle trajectory paths. Numerical integration was used to compute the trajectories. FIG. 3. Examples of rrf trap trajectory in the testing frame. With x=1, y=0, dx/d =0, and dy/d =0 as initial conditions, these trajectories are numerically generated using the fourth-order Runge-Kutta technique from =0 to 100. The particle is unstable in c and d, but it is trapped in a, b, and e. Figure 2 displays the q and d parameter values. A big circular secular motion and a little micromotion are particularly noticeable in a. When 1+=0 for e, the parameter values are selected so that the 1+ secular motion is merely a displacement from the trap centre. Eqs. 6 and 7 are

analytical solutions that may have been employed instead of the fourth-order Runge-Kutta technique. Particularly in Fig. 3a, a large-radius secular motion with a tiny circular micromotion that resembles a particle in a lrf trap can be noticed. We set d=2 +21+q2 in Fig. 3e, where 1+=0 and the corresponding motion are displaced from the trap's centre.

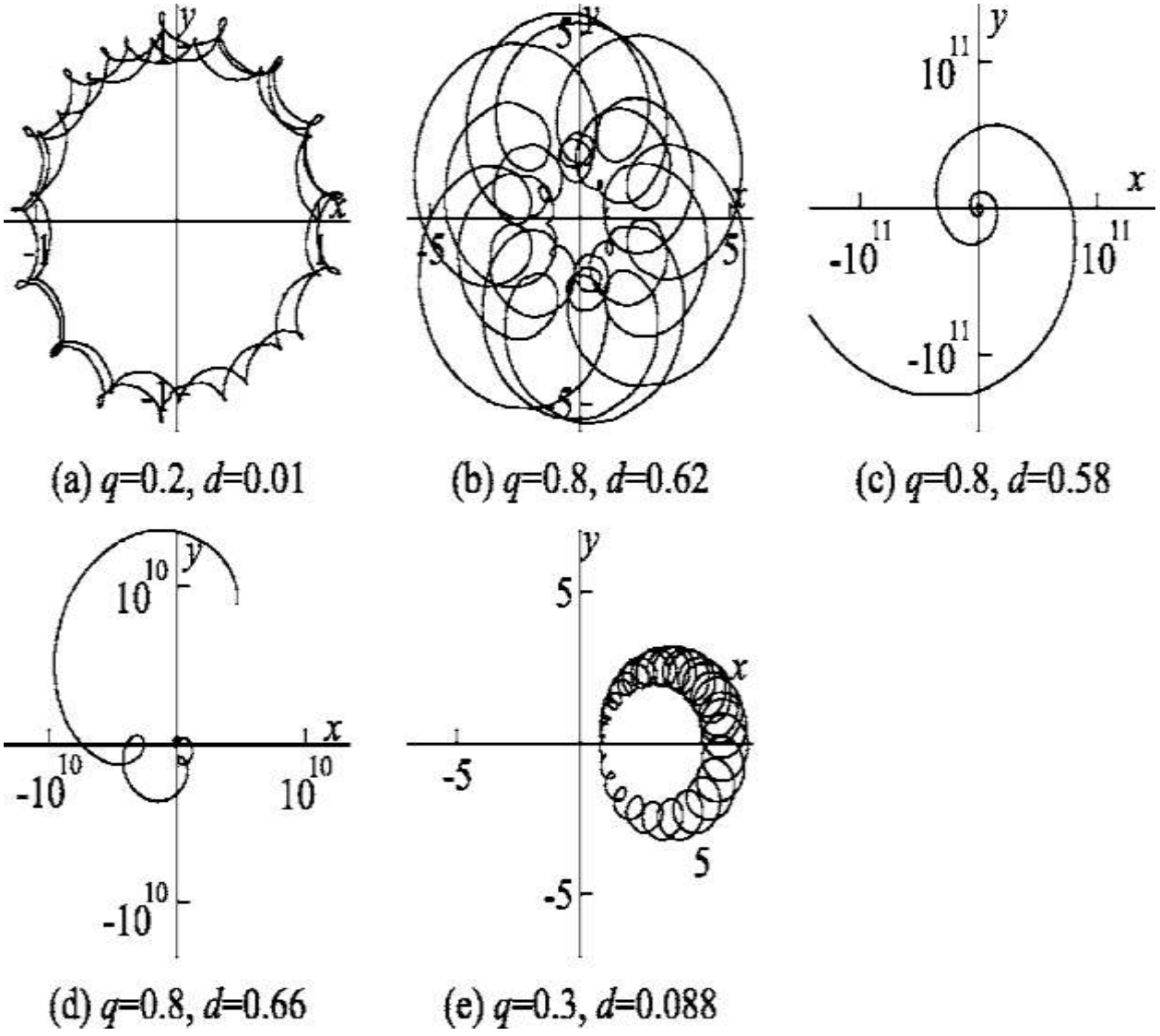


**(111) A ROTATING-RF TRAP With Particular Motion :**

The motion of a charged particle in a rrf trap for weak driving amplitudes corresponding to q2 1 is covered in this section. Even though we have the precise answers for a rrf trap, this approximation will help us comprehend the dynamics. A pseudo potential approximation performs well in this domain in a lrf trap. In other words, the confining force caused by the inhomogeneous rf fields may be calculated from a potential known as the pseudopotential on time scales that are longer than the duration of the rf

drive. The pseudo potential for the lrf trap is cylindrically symmetric and is identified by a frequency known as the secular frequency. The lrf q2/2d1 formula yields the lrf trap secular frequency for q21. The slow secular motion and the quick micromotion at multiples of the rf driving frequency 2 in normalised units are superimposed to form the general motion. To second order in *q* and _*q*2−*d*, and to first order in *d*, the characteristic frequencies of Eq. _13_ are given by

$$\omega_{1+} \sim \sqrt{q^2 - d} - \frac{q^2}{2},$$

$$\omega_{2+} \sim -\sqrt{q^2 - d} - \frac{q^2}{2},$$

$$\omega_{1-} \sim -2 - \sqrt{q^2 - d} + \frac{q^2}{2},$$

$$\omega_{2-} \sim -2 + \sqrt{q^2 - d} + \frac{q^2}{2}. \qquad (14)$$

Expanding the _*j*'s to first order in small parameters, the laboratory-frame solutions of Eq. _10_ become

$$x \sim \sum_{j=1,2} [(2-q)A_j \cos(\omega_{j+}\tau + \phi_j) + qA_j \cos(\omega_{j-}\tau - \phi_j)],$$

$$y \sim \sum_{j=1,2} [(2-q)A_j \sin(\omega_{j+}\tau + \phi_j) + qA_j \sin(\omega_{j-}\tau - \phi_j)]. \qquad (15)$$

We can show that two generally nondegenerate circular secular movements have frequency of 1+ and 2+. The driving frequency 2 in the normalised units of Eqs. 2-4 is roughly equivalent to 1=2 1+ and 2=2 2+. The frequency of two circular micromotions is what they are as a result.

The micro motion's radius is q/2 times smaller than the secular motion's radius. Equation 14 demonstrates that the secular frequencies are q2d to first order. The two secular movements are therefore degenerate in this lowest-order approximation, which corresponds to circular motions with the same frequency but in the opposite direction. Similar to the lrf trap, but with a 2 greater secular frequency for the same q, or the same amplitude and frequency of the applied ac field. The degeneracy of the secular frequencies, however, is broken in second order in the rrf trap. The secular frequencies

for the x and y motion are degenerate to all orders of q and d in the lrf trap, in contrast. A charged particle in a rrf trap experiences a precession in its motion at a frequency of q2/2, which is caused by the breakdown of the degeneracy of the secular frequencies. Let x in Eq. 15 equal X + xm and y equal Y + ym, where X and Y are the j+ terms for the secular motion and xm and ym are the j terms for the micromotion, respectively. Take into account simply the secular motion, for instance if the particle's secular motion has the following coordinates: X=1, Y=0, X =0, and Y =0. Keeping first-order contributions to the amplitudes but just second-order contributions to the characteristic frequencies, we obtain

$$X + iY = e^{-i(q^2/2)\tau}\left(\cos\sqrt{q^2 - d}\tau + i\frac{q^2}{2\sqrt{q^2 - d}}\sin\sqrt{q^2 - d}\tau\right) \quad (16)$$

for the secular motion of the particle. Equation _16_ describes an elliptical particle orbit with aspect ratio of *q*2 / _2_*q*2−*d*_ that precesses about the *z* axis at a frequency *q*2 /2 in the −_ ˆ direction. By simulating Eqs. 2 and 3 numerically, the precession may also be shown. For q = 0.2 and various values of d, the particle orbits predicted using the fourth-order Runge-Kutta technique are shown in Figure 4. Similar beginning conditions for the secular motion used to calculate Eq. 16 are provided by the initial conditions x=1, y=0, x=0, and y=q for the total particle motion secular plus micromotion. The particle orbit precesses by around 120° 2.1 rad from 0 to 100, which is consistent with the theoretical prediction of q2/2 = 2 radians. The differing radii of the micromotion linked to the two distinct secular movements are what cause the degeneracy of the secular frequencies to break. The coefficients 1+ j in Eq. 10 may be calculated to second order in q to directly witness this. Because they correspond to distinct movements with respect to the spinning quadrupole field, these two secular motions are not equal in terms of physics. The circular motion in the same direction as the rotating field that the 2+ secular motion represents revolves around the trap axis in the direction. The 1+ secular motion for an axially weak trap dq corresponds to a circular motion that resists the rotating field. We can easily demonstrate that the Coriolis force is mostly to blame for the difference in the radii of the two micromotions with an axially weak trap dq and a weak rf drive q21. Consider the scenario in which Eq. 10's A10 and A2=0 are stimulated by the 1+ secular motion alone and are transformed into a frame rotating with 1+. The quadrupole potential in this frame spins with frequency 11+ about the z axis.

The electric field spins with a frequency of 221+ at the particle site since this is a quadrupole potential. At the same frequency, this revolving electric field generates a circular motion.

For a weak rf drive, the centrifugal potential in the 1+ spinning frame is q2, and it may be disregarded. Thus, as seen in Fig. 5, the particle motion is primarily made up of circular motion with a frequency of 221+. The forces FE1 resulting from the rotating field and FC1 resulting from the transition to the 1+ rotating frame work together to define the radius 1 of the micromotion.

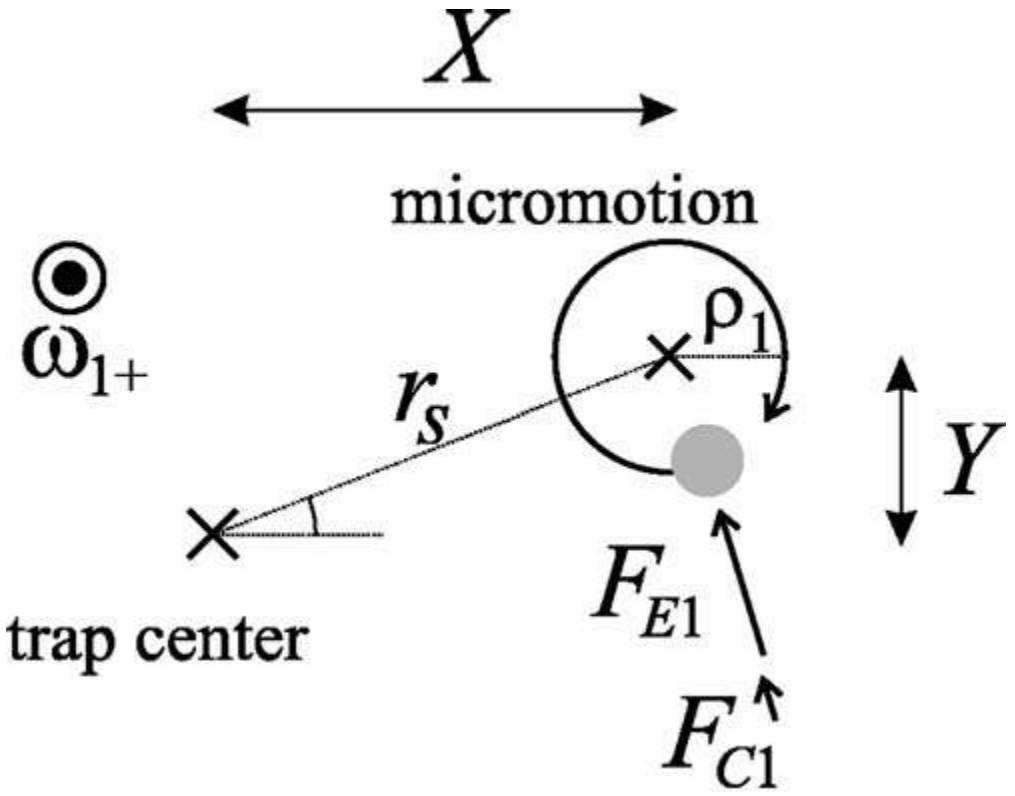


FIG. 5 is a schematic illustration of a particle moving in a frame that is spinning at 1+ and the forces acting on it. The electric field force and the Coriolis force are denoted by FE1 and FC1, respectively.

$$F_{E1} = -2qr_s,$$

$$F_{C1} = 2\omega_{1+}(-2-2\omega_{1+})\rho_1 \sim -4\omega_{1+}\rho_1. \qquad (17)$$

Here, rs is the micro motion's cylindrical radius, and a negative force indicates that it is pointing in the direction of the micro motion's centre. The relationship FE1+FC1=221+21 41+21+1 is required for circular motion with radius 1.

$$\rho_1 = \frac{qr_s}{2(1+\omega_{1+})} \sim \frac{qr_s}{2}(1-\omega_{1+}). \qquad (18)$$

This demonstrates how the radius of the micromotion is dependent on the secular frequency owing to the Coriolis force. 1 is decreased by 1+ for the 1+ secular motion. The micromotion radius for the 2+ secular motion is enlarged by 2+ because it spins in the opposite direction from the 0 and 2 secular motions. A bigger secular restorative force is produced by a larger micromotion radius. For instance, we may write the 1+ secular and associated micromotions in the laboratory frame and within the approximations of Eq.

$$x+iy = X+iY+\frac{q(1-\omega_{1+})}{2}(X-iY)e^{-2i\tau}. \qquad (19)$$

$$\frac{d^2}{d\tau^2}(X+iY) = [d-q^2(1-\omega_{1+})](X+iY). \qquad (20)$$

The coefficients on the right-hand side must be 1+ 2 since Eq. 20 is the equation for the secular motion. As a result, we get at 1+q2dq2 /2, and it would seem that the plus sign should be used. The same equation also applies to 2+, hence the negative sign is used for 2+. When d>> q, this result corresponds with Eq.

## (4) MODIFICATIONS OF ROTATING-rf TRAPS

### A. Uniform magnetic field :

As demonstrated in Section II, the radial motion of a particle is still characterized by four Fourier components in the presence of a homogeneous magnetic field in the z direction. The proper name for this trap is a rrf Penning trap. A rrf Penning trap's stability criteria were already established in Eq. 9 and in Ref.[27] this instability is due to parametric excitation of a Penning trap motional frequency by the applied rotatin quadrupole electric field. The case of ___*m* was investigated in detail experimentally in Ref. The eigenfrequencies in a rrf Penning trap are given by the λ_*j*±. _λ_*j*±=−1±ω_*j* where the _*j* are given by Eq _8_._ For the special case of *q*=0, these become _when __ω2

$$\omega_{1+} = -\frac{\mu}{2} + \frac{1}{2}\sqrt{\mu^2 - 4d},$$

$$\omega_{1-} = -2 + \frac{\mu}{2} - \frac{1}{2}\sqrt{\mu^2 - 4d},$$

$$\omega_{2+} = -\frac{\mu}{2} - \frac{1}{2}\sqrt{\mu^2 - 4d},$$

$$\omega_{2-} = -2 + \frac{\mu}{2} + \frac{1}{2}\sqrt{\mu^2 - 4d}. \qquad (21)$$

Hence The modified cyclotron frequency in a Penning trap is 2+, and 1+ is the magnetron frequency expressed in normalised units. Because the amplitudes of these motions, 1+ j Eq. 10, are zero if q=0, there is no motion corresponding to 1 or 2, respectively. The modified cyclotron frequency in the case of 2 is 1 and the magnetron frequency is 2.

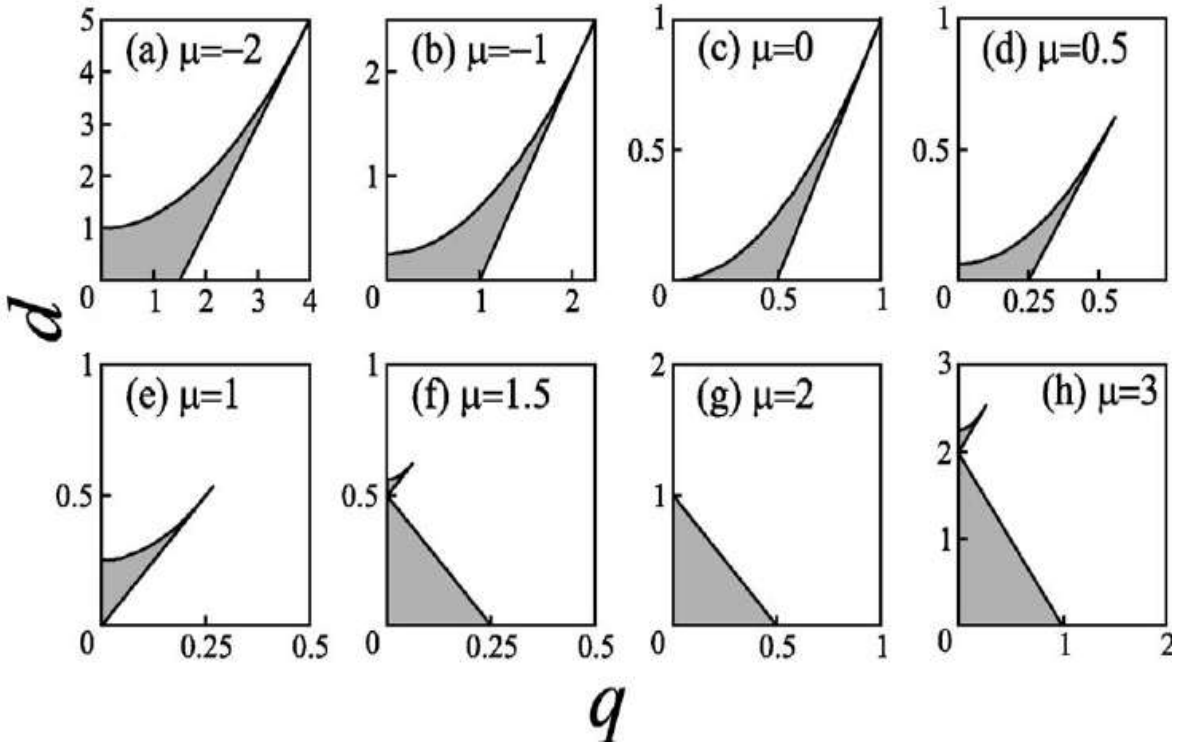


FIG. 6. Stability diagrams in the *q*-*d* plane for some specific values of μ. The case of μ =0(c) is the same as Fig. 2.

### B. Static quadrupole potential

Mass spectroscopy is one of the crucial uses for rf traps. Most typically utilised as a quadrupole mass filter QMF 15,16 is the lrf trap in the limit d=0. In addition to the oscillating quadrupole field, a static quadrupole field determined by the formula Vsx2y2 / rr 2 is used for mass spectroscopy. Mass spectroscopy is typically accomplished by adjusting the rf frequency while keeping the voltages of the static and rf quadruples constant to confine charged particles whose charge-to-mass ratio lies within a particular range Here, we analyse the scenario where an additional static quadrupole potential (Vsx2y2/rr2) is applied to the spinning rf. a rrf trap's field. We simply take =d=0 into account. The formulas for motion become

$$\frac{d^2x}{d\tau^2} = -2qx\cos 2\tau + 2qy\sin 2\tau - ax,$$

$$\frac{d^2y}{d\tau^2} = 2qy\cos 2\tau + 2qx\sin 2\tau + ay, \qquad (22)$$

where *a* is a dimensionless parameter defined as 2*eVs* /*mrr* 2_2. Eq. 22 is no longer made simpler by changing the variables x, y, and in Eq. 6 to. Therefore, Mathieu-type functions must be used to represent movements in this trap. A two-dimensional analysis similar to the one used for Mathieu equations 24 can be utilised to find the solutions. The Appendix displays specifics of this analysis. The stability diagram of a rrf QMF in the q-a plane is obtained from the analysis in the Appendix and is shown in Figure 7. In this picture, we also provide the stability diagram of a lrf QMF for comparison. In contrast to the lrf QMF, which has extra tiny stability zones around, say, a=3 and q=3, the rrf QMF lacks higher order stability criteria. Mass spectroscopy could benefit from the rrf QMF's simplified stability diagram. Additionally, the range of q in the stability zone of the rrf QMF is less than that of the lrf QMF. As a result, lower values of q can be used to run the rrf QMF. As a result, there may be certain benefits for mass spectroscopy. For instance, because q is proportional to 1/m, the top limit of the mass range of a rrf QMF can be larger than that of a lrf QMF.

## V. CONCLUSIONS

We've spoken about a design for a rotating-rf trap in which the ion motion is accounted for by straightforward trigonometric functions. For instance, this straightforward ion motion could be more beneficial than that of a lrf trap in creating motional sidebands of optical spectral lines that are simpler for trapped ions to produce. The study of this trap's quantum mechanics may be made simpler by the simplicity of the classical motion in a rrf trap. The only variety of rf trap that is not described by a Mathieu-type solution, as far as we are aware, is the rrf trap. Two circular secular movements and two related circular micromotions make up a particle's motion in a rrf trap. One of the secular movements for an axially weak trap dq rotates in the opposite direction from the rotating field, whereas the other secular motion rotates in the same direction. The absolute values of the secular frequencies differ by an order of q2, and this disparity causes the secular motion to precess. In a rrf trap with the identical trap settings, the secular frequency is 2 times more than in a lrf trap. Consequently, a rrf trap can provide tighter confinement. The motion may still be characterized by trigonometric functions even when a uniform magnetic field is provided along the trap axis.

But to characterize the mobility of the ions in a static quadrupole electric field, Mathieu-like functions are needed. We got the stability diagram of a static quadrupole field rrf quadrupole mass filter. The single stability area of the rrf QMF, which exists for smaller values of q, may provide it some benefits over the lrf QMF.

## Reference

1_ M. D. Barrett, J. Chiaverini, T. Schaetz, J. Britton, W. M.Itano, J. D. Jost, E. Knill, C.Langer, D. Liebfried, R. Ozeri,and D. J. Wineland, Nature _London_ **429**, 737 _2004_.

2_ J. I. Cirac and P. Zoller, Phys. Rev. Lett. **74**, 4091 _1995_.

3_ J. Pachos and H. Walther, Phys. Rev. Lett. **89**, 187903 _2002_.

4_ H. Häffner, S. Gulde, M. Riebe, G. Lancaster, C. Becher, J.Eschner, F. Schmidt-Kaler, and R. Blatt, Phys. Rev. Lett. **90**,143602 _2003_.

5_ J. D. Prestage, G. J. Dick, and L. Maleki, J. Appl. Phys. **66**,1013 _1989_.

6_ J. C. Bergquist, S. R. Jefferts, and D. J. Wineland, Phys. Today**54** _3_, 37 _2001_.

7_ G. P. Barwood, H. S. Margolis, G. Huang, P. Gill, and H. A.Klein, Phys. Rev. Lett. **93**, 133001 _2004_.

8_ A. A. Madej, J. E. Bernard, P. Dube, L. Marmet, and R. S.Windeler, Phys. Rev. A **70**, 012507 _2004_

9_ Chr. Tamm, D. Engelke, and V. Bühner, Phys. Rev. A **61**,053405 _2000_.

10_ D. H. E. Dubin and T. M. O'Neil, Rev. Mod. Phys. **71**, 87
1999_.

11_ W. M. Itano, J. J. Bollinger, J. N. Tan, B. Jelenković, X.-P.Huang, and D. J. Wineland, Science **279**, 686 _1998_.

12_ L. Hornekaer and M. Drewsen, Phys. Rev. A **66**, 013412

2002_.

13_ J. Estrada, T. Roach, J. N. Tan, P. Yesley, and G. Gabrielse,Phys. Rev. Lett. **84**, 859 _2000_.

14_ P. Paasche, T. Valeuzuela, D. Biswas, C. Angelescu, and G.

Werth, Eur. Phys. J. D **18**, 295 _2002_.

15_ W. Paul and H. Steinwedel, Z. Naturforsch. A **8**, 448 _1953

16_ P. K. Ghosh, *Ion Traps* _Clarendon, Oxford, 1997_.

17_ D. J. Wineland, W. M. Itano, and J. C. Bergquist, Opt. Lett.**12**, 389 _1987_.

18_ F. Diedrich and H. Walther, Phys. Rev. Lett. **58**, 203 _1987_.

19_ T. Sauter, W. Neuhauser, R. Blatt, and P. E. Toschek, Phys.Rev. Lett. **57**, 1696 _1986_.

20_ W. Paul, Rev. Mod. Phys. **62**, 531 _1990_.

21_ W. Paul, in Laser Manipulation of Atoms and Ions,*Proceedings of the International School of Physics* "Enrico Fermi," Course 118, 1991, edited by E. Arimondo, W. D. Phillips,and F. Strumia, _Elsevier, Amsterdam, 1992_.

22_ R. I. Thompson, T. J. Harmon, and M. G. Ball, Can. J. Phys. **80**, 1433 _2002_.

23_ R. F. Wuerker, H. Shelton, and R. V. Langmuir, J. Appl. Phys. **30**, 342 _1959_.

24_ N. W. McLachlan, *Theory and Application of Mathieu Functions*Clarendon, Oxford, 1947_.

25_ X. -P. Huang, F. Anderegg, E. M. Hollmann, C. F. Driscoll, and T. M. O'Neil, Phys. Rev. Lett. **78**, 875 _1997_.

26_ X. -P. Huang, J. J. Bollinger, T. B. Mitchell, W. M. Itano, andD. H. E. Dubin, Phys. Plasmas **5**, 1656 _1998_.

27_ T. Hasegawa, M. J. Jensen, and J. J. Bollinger, Phys. Rev. A**71**, 023406 _2005_.

28_ The stability diagram of a lrf trap with nonzero *d* is just thestability of a single one-dimensional Mathieu equation, because

the equation of motion in *x* is identical to that in *y* exceptfor the sign of *q*, which does not affect the stability.

29_ L. S. Brown and G. Gabrielse, Rev. Mod. Phys. **58**, 2331986_.